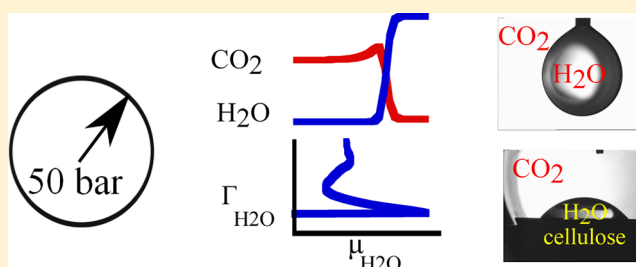


Interfacial Tension and Wettability in Water–Carbon Dioxide Systems: Experiments and Self-consistent Field Modeling

Soumi Banerjee,^{*,†} Eveline Hassenklöver,[‡] J. Mieke Kleijn,[†] Martien A. Cohen Stuart,[†] and Frans A. M. Leermakers^{*,†}[†]Laboratory of Physical Chemistry and Colloid Science, Dreijenplein 6, Wageningen University, 6703 HB, Wageningen, The Netherlands[‡]Technical University Hamburg-Harburg, Process Engineering II, Heat and Mass Transfer, Eißendorfer Str. 38, 21073, Hamburg, Germany

S Supporting Information

ABSTRACT: This paper presents experimental and modeling results on water–CO₂ interfacial tension (IFT) together with wettability studies of water on both hydrophilic and hydrophobic surfaces immersed in CO₂. CO₂–water interfacial tension (IFT) measurements showed that the IFT decreased with increasing pressure and the negative slopes of IFT–pressure isotherms decreased with increasing temperature. Water contact angle on a cellulose surface (hydrophilic) immersed in CO₂ increased with pressure, whereas the water contact angle on a hydrophobic surface such as hexamethyl disilazane (HMDS) coated silicon surface was almost independent of pressure. These experimental findings were augmented by modeling using the self-consistent field theory. The theory applies the lattice discretization scheme of Scheutjens and Fleer, with a discretization length close to the size of the molecules. In line with this we have implemented a primitive molecular model, with just small variations in the molar volume. The theory makes use of the Bragg-Williams approximation and has binary Flory–Huggins interaction parameters (FH) between CO₂, water, and free volume. Using this model, we generated the complete IFT–pressure isotherms at various temperatures, which coincided well with the trends reported in literature, that is, the water–CO₂ interfacial tension decreased with increasing pressure for pressures ≤ 100 bar and became independent of pressure > 100 bar. The transition point occurred at higher pressures with increasing temperature. At three-phase coexistence (water–CO₂–free volume) and at the water–vapor interface (water–free volume), we always found the CO₂ phase in between the water-rich and free volume-rich phases. This means that for the conditions studied, the water–vapor interface is always wet by CO₂ and there are no signs of a nearby wetting transition. Calculation of the water contact angle on a solid surface was based on the computed adsorption isotherms of water from a vapor or from a pressurized CO₂-rich phase and analysis of surface pressures at water–vapor or water–CO₂ coexistence. The results matched reasonably well with the experimental contact angle data. Besides, we also computed the volume fraction profiles of the CO₂, H₂O, and the V phase, from which the preferential adsorption of CO₂ near the hydrophilic surface was deduced.



■ INTRODUCTION

Interfacial tension and wettability of water–CO₂ (gaseous, liquid or supercritical) systems are important for many industrial processes, such as Geological storage,^{1–3} dry-cleaning,⁴ oil recovery⁵ and fluid extractions.⁶ Hence, it is necessary to understand the molecular origin of CO₂–water interfacial tension (IFT), influence of pressure and temperature on IFT and contact angles. Subject to the temperature and pressure range, several interfaces such as gaseous CO₂–liquid water, liquid CO₂–liquid water and supercritical CO₂–liquid water come into play at the various stages of the above-mentioned processes.

Experimental CO₂–water IFT data, measured by various research groups^{1,7–13} and including the present study, show a decrease of IFT with pressure. Contact angle measurements under similar conditions are rare,¹⁴ probably because of the

difficulty involved in the measurement, even though wetting plays a significant role in all those above-mentioned processes. This brings us to the development of a molecular model for water–CO₂ system to gain molecular insight into the physics of the processes at one hand and on the other hand deepen the insight about the interfacial properties of CO₂/water systems covering the relevant pressure range.

To date there have been only a few attempts^{11,15–19} to predict the IFT and thermodynamic properties of the CO₂–water interface and these are mainly based on (n, P, T) and (n, V, T) molecular dynamics and Monte Carlo simulations, in which the IFT is computed from integrating the difference

Received: January 28, 2013

Revised: June 13, 2013

Published: June 20, 2013

between the normal and tangential pressure components across the interface. These simulations are still reasonably inexpensive (involving reasonable CPU time) to compute a particular interfacial tension corresponding to a specific pressure and temperature condition. However, prediction of IFT subject to a large pressure range imposes long CPU time for a sufficiently large system size (for a reasonable accuracy of the calculated IFT, a good system size would consist of $\geq 10^6$ molecules). One issue is that the interface will fluctuate in shape and in simulations it is expensive to allow for this. The interfacial tension should incorporate these fluctuations. This feature of MD simulation makes it even more unattractive to study systems consisting of more than one interface such as the present system. This problem becomes more severe for multicomponent systems, that is, systems that feature amphiphiles that may self-assemble in CO_2 . In this study, we develop an alternative type of modeling of such systems.

Following the work of van der Waals and Cahn and Hilliard,²⁰ an equation of state based model in combination with density gradient theory has been employed recently to model CO_2 –water² and alkane systems.²¹ In this approach, the equation of state was employed to calculate the Helmholtz energy of water– CO_2 mixtures and using a so-called influence parameters coupled with the density gradients of the two components led to a reasonable fit of the IFT data.² However, it should be noted that since the influence parameters were used as fitting parameters to match the experimental and the theoretical IFT– P isotherms, this method potentially hides problems that should be traced to the mean field approximation or the approximate models used. The density gradient theory may be extended to account for more complicated situations, but then this approach becomes definitely more involved.

In this paper, we focus on an even more primitive mean field model with a regular solution-based equation of state. More specifically, we follow the self-consistent field (SCF) theory making use of the lattice discretization scheme of Scheutjens and Fleer (SF).^{22,23} In the model the molecules occupy an integer number of lattice sites. The segments are freely jointed, which allows for an efficient way of computing entropic contributions resulting from the many possible configurations of the molecules on the lattice. We chose this approach because it had been applied before to describe self-assembly of amphiphiles, so it naturally fits in with our ambition to model, in a follow-up study, amphiphiles in water– CO_2 systems. Here we focus on systems that do not yet feature such amphiphiles. We hasten to mention that our mean field approach is subject to the same criticism as for the gradient theory mentioned above. That is why we have not pushed the fitting to its limits.

Here we will show that the SF-SCF theory can be applied to systems that have small molecules such as CO_2 and water. Again, the lattice approximation prevents an accurate account for the molecular details, which unavoidably leads to a qualitative rather than quantitative description. Interfacial tensions (captured in the grand potential per unit area of an interface) can be computed in SCF by knowing the volume fractions, the complementary segment potential profiles and all binary (Flory–Huggins) interaction parameters.²⁴ The water contact angle on a solid substrate can be extracted from the analysis of the computed adsorption isotherms of water either from a CO_2 –vapor phase, or from a pressurized CO_2 fluid, as explained in more detail below. One of the goals of this paper is to find a set of interaction parameters, which for the CO_2 –

water–free volume system reproduces approximately the phase behavior and the interfacial tensions. The same model is then carried further to study the water contact angle in liquid CO_2 (and in future will be used to study surfactant self-assembly in these systems). Comparison with experimental data will be informative about the physico-chemical behavior of the mimicked surfaces.

The paper is organized in the following way: we first present the experimental data of water– CO_2 IFT and water contact angles on hydrophilic and hydrophobic surfaces with respect to CO_2 activity at pressures and temperatures relevant for the dry-cleaning process. This is followed by a description of the SF-SCF theory, focusing on the (primitive) molecular model that is used. The experimental and modeling results are presented together in such a way that we consider systems with increasing complexity. Correspondence to the experimental data has directed us to particular choices for the various interaction parameters that we mostly motivate *a posteriori*. As usual, at the end of the paper we will summarize our conclusions.

MATERIALS AND METHODS

Preparation of Cellulose and HMDS-modified Silica Surfaces. Silicon wafers (WaferNet) with a 3 nm surface oxide layer were cut into small pieces of 0.5 cm \times 2 cm using a diamond craft knife. The wafers were sonicated in water and subsequently in ethanol, each for 15 min. After this the wafers were cleaned using a plasma cleaner for 10 min and the cellulose layers were spin-coated on the wafers and hydrolyzed.^{25,26} After coating, the layers were oven-dried at 373 K for 1 h and their thickness was measured using an ellipsometer. The hydrophobic silica surfaces were prepared by exposing silica surfaces to hexamethyldisilazane (HMDS) vapor in a desiccator for at least 24 h. Before closing the desiccator, nitrogen was purged to prevent HMDS to react with the moisture present in the air. The modified strips were washed with toluene, ethanol and acetone. The strips were finally dried using nitrogen flow. The IRRAS spectrum of the modified and unmodified surfaces are given in Figure S1 in the Supporting Information. The modified HMDS surface clearly contains methyl-rich domains compared to the unmodified surface.

Measurement of Interfacial Properties in Liquid CO_2 . Water (deionized)–liquid CO_2 (Westfalen Gas, purity 99.5%) interfacial tension and contact angle measurements were done using a high pressure view cell having two transparent windows. A schematic of the instrument can be found in ref 13. The interfacial tension and contact angles were measured using the pendant drop and sessile drop methods respectively, where in the former case a water drop was generated at the end of a steel capillary and in the latter a water drop was placed on a solid surface of interest. In both cases a CCD camera recorded the image of these drops and the analyses of drop shapes were done using the DSA software (Kruss, GmbH). A description of the pendant drop technique can be found in references.^{1,10}

Theory. As mentioned in the introduction, we used a mean field approach implementing the lattice discretization scheme as proposed by Scheutjens and Fleer.^{22,23} More precisely, we implemented a so-called lattice gas model, similar to regular solution theory.²⁷ On this lattice molecules are placed, which are composed of (an integer number of) monomeric units called segments. A segment exactly fits on one lattice site. Hence, both are characterized by a linear length a . Degrees of freedom at length scale smaller than a are not taken into consideration. In the lattice we recognize layers, numbered $z =$

$1 \cdots M$ and each layer has L sites. Formally $L \rightarrow \infty$, and fluctuations in composition within a lattice layer are ignored (mean-field approximation). This allows us to normalize, e.g., the free energy, by L and thus to focus on the free energy per unit area (that is per a^2) as the leading thermodynamic quantity. On the lattice there are two molecular species: water ($i = 1$) and CO_2 ($i = 2$) and there are unoccupied lattice sites. Such a model may be referred to as a two-component compressible model. It features chemical potentials μ_i for the molecular components and a pressure P as the intensive parameters (on top of the entropy). It is possible to map this model onto a three-component incompressible model, wherein the “free volume” sites are interpreted as being composed of a new (monomeric) species. In such a three-component model, the system is incompressible: all lattice sites are occupied by either water ($i = 1$), CO_2 ($i = 2$) or free volume ($j = 3$). In this system, we have three chemical potentials $\tilde{\mu}_j$, and the system is incompressible as the volume is not a free variable. The calculations and the presentation of the SF-SCF theory typically is done in the context of the incompressible model, but below we will report the results in terms of the compressible model. The mapping rules are:

$$\mu_1 \leftrightarrow \tilde{\mu}_1 - N_1 \tilde{\mu}_3 \quad (1)$$

$$\mu_2 \leftrightarrow \tilde{\mu}_2 - N_2 \tilde{\mu}_3 \quad (2)$$

$$Pa^3 \leftrightarrow -\tilde{\mu}_3 \quad (3)$$

where N_1 is the number of lattice sites occupied by a single molecule water, and N_2 represents the molar volume (in lattice sites) for CO_2 , as will be elaborated below.

Volume fractions, $\varphi_i(z)$, are the natural concentration units of species i in layer z . These are related to the actual number concentrations, c

$$\varphi_i(z) = c_i(z)a^3 = \frac{n_i(z)}{L} \quad (4)$$

where $n_i(z)$ represents the number of monomers of type i in layer z . Typically we use volume fractions and reserve the number of molecules of molecule i to refer to the system, that is, $n_i \equiv \sum_z \varphi_i(z)/N_i$ from which it is understood that the number of molecules is normalized by L .

For bulk-phase behavior, we have implemented mirror-like boundary conditions. This means that we impose

$$\varphi_i(0) = \varphi_i(1) \quad (5)$$

$$\varphi_i(M+1) = \varphi_i(M) \quad (6)$$

or in other words, we assume that there are no gradients in density across the boundaries of the system.

In some of our calculations, we are interested in the interaction of the molecular species with a substrate. In this case, we replace the boundary condition at the lower bound by setting the volume fractions of all molecular species equal to zero at layer $z = 0$. The substrate on the other hand will have the volume fraction unity in layer $z = 0$.

Molecular Detail. The molecular description of the three types of molecules is explained in Figure 1. Water is represented as a cluster of 5 segments,²⁸ W_5 , with $N_1 = 5$ to take into account (admittedly very approximate) H-bonded interactions. The architecture is such that one central W segment is (permanently) surrounded by four neighbors. CO_2

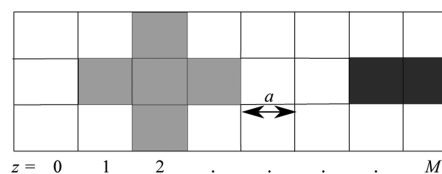


Figure 1. Two-dimensional representation of a lattice filled with three species: ($i = 1$) water, (filled gray \square) represented as clustered pentamers, ($i = 2$) CO_2 as dimer (filled black \square) and ($i = 3$), free volume as a monomeric unit (unfilled \square). The lattice parameter a is indicated.

is represented as a dimer, D_2 , with $N_2 = 2$ and the free volume as a single entity, V_1 , with $N_3 = 1$.

In our adsorption study, we impose the volume fraction of the solid phase S as follows:

$$\varphi_s(z) = \begin{cases} 1 & z = 0 \\ 0 & z > 0 \end{cases} \quad (7)$$

At this stage it is good to mention that this molecular representation inherently brings in asymmetry in the system as the overall interactions are determined by the individual and cross-interactions among three different types of species, differing in segment numbers N_i as well as in architecture. The conformational degrees of freedom are evaluated by the freely jointed chain (FJC) model^{29–31} as will be elaborated below, that is, where the SCF machinery is outlined.

Interaction Parameters. Interactions between CO_2 , water and free volume give rise to thermodynamic properties of the system. These interactions are, for incompressible systems, conveniently specified by Flory–Huggins (FH) interaction parameters specified on the segment level, more specifically for segments A and B by

$$\chi_{AB} = \chi_{BA} = \frac{Z}{2k_B T} [2U_{AB} - U_{AA} - U_{BB}] \quad (8)$$

where Z is the lattice coordination number ($Z = 6$ for a cubic lattice), and $k_B T$ the thermal energy. It is easily seen that the χ parameter is zero for like contacts, that is $\chi_{AA} = 0$. For J species in the incompressible system, we need $J \times (J - 1)/2$ different χ values to fully specify the interaction set. Note that there are J reference values in this case.

In a compressible lattice gas model it is, arguably, more intuitive to choose the interactions U_{AB} as the natural parameters and take the interactions with the free volume component to be zero. Then there are $J - 1$ molecular components and thus it suffices again to specify $((J - 1)^2 + (J - 1))/2 = J(J - 1)/2$ different parameters. Indeed, we can “translate” the set of χ parameters (one-to-one) into the set which takes the interactions with free volume to be zero. As the SCF theory is most easily elaborated in the incompressible system, we choose to report the corresponding FH-parameters.

In Table 1 we have summarized the parameters assigned to each unlike (and like) interaction between the segments. We would like to stress that with our model we focus more on understanding qualitative trends and molecular mechanisms rather than exactly matching the experimental data. The rationale behind the chosen values will be briefly elaborated.

From the Flory–Huggins theory one can find a critical χ^{cr} above which in a system with two molecular components A and B, having a molar volume $N_A a^3$ and $N_B a^3$, a solubility gap exists.

Table 1. Interaction Parameters χ between Various Pairs at 313 K^a

χ	D	W	V	S_c	S_m
D	0	1.5	1.5	-3.6	-1.91
W	1.5	0	3.5	-4.5	-0.91
V	1.5	3.5	0	0	0
S_c	-3.6	-4.5	0	0	
S_m	-1.91	-0.91	0		0

^aHere D is the monomer in CO₂, W is the monomer in water, V is the empty site, S_c is the cellulose and S_m is the HMDS-modified silica.

$$\chi_{AB}^{cr} = \frac{1}{2} \left(\frac{1}{\sqrt{N_A}} + \frac{1}{\sqrt{N_B}} \right)^2 \quad (9)$$

Focusing on the parameters for D , W and V , we have to choose χ_{DW} , χ_{DV} and χ_{VW} above their critical values, being 0.67, 1.46 and 1.05, respectively. Even then, the question remains how far the chosen χ should be above the χ^{cr} . We can make educated guesses. For example we know that water-free volume is very far from critical and therefore we used a value of $\chi_{VW} = 3.5$. This value leads to a value of the water-vapor interfacial tension which is close to the experimental one. Similar considerations apply for the other two binary parameters. The CO₂-vapor is much closer, indeed relatively close to critical and we settled for $\chi_{DV} = 1.5$ accordingly. The value of χ_{DW} was selected to reproduce the value of the interfacial tension between liquid CO₂ and water. Interestingly this gave a value of 1.5. Inspection shows that this value, even though numerically the same as for CO₂ and V , it is reasonably far from critical.

So far we have discussed the selection of χ parameters for the CO₂-water system. To describe the wetting phenomena on hydrophilic and hydrophobic surfaces we need additional FH parameters. Our choices are also listed in Table 1. Basically because the surface component has a fixed and specified volume fraction profile, one can select one species for which the surface interactions can be set to zero. Other interactions are then counted with respect to this reference. For obvious reasons, we have chosen to assign the surface-free volume interaction parameter to zero, leaving two χ parameters, i.e., surface-CO₂ and surface-water, to be specified.

Although data fitting was not intended, we succeeded in reproducing the correct trends of the CO₂-water interfacial tension and water contact angles as a function of pressure. We also attempted to understand the effect of temperature on interfacial tension or contact angle. From comparison with experimentally found trends, it was decided that parameters in Table 1 correspond to $T = 313$ K. Unless mentioned otherwise, we use eq 8 to compute the interactions parameters for other temperatures, implying that we have interpreted the FH parameters as purely enthalpic in nature. This means that with increasing temperature the interactions become less repulsive.

SCF Equations. Formally, the SCF theory can be introduced by starting with an appropriate free energy expression that can be written in terms of the volume fraction profiles $\varphi_i(z)$ and the complementary segment potential profiles $u_i(z)$. The segment potential may be interpreted as the work needed (in units of $k_B T$) to bring a segment from the bulk (where the potential is zero) to the coordinate z . Optimising the free energy both with respect to the volume fractions and the segment potentials leads to the mutually

dependence of these two profiles: the volume fractions can be computed from the potentials and vice versa. Clearly, these two profiles should be consistent with each other and the self-consistent field solution is found numerically by an iterative procedure. Here we do not go into these details. Instead we state the resulting equations.

The segment potentials u_A , with $A = D, W, V$ are given by

$$u_A(z) = \alpha(z) + \sum_B \chi_{AB} (\langle \varphi_B(z) \rangle - \varphi_B^b) \quad (10)$$

Here the summation over the segments B include the surface component (if present). The volume fraction in the bulk is denoted by the super index b . The angular brackets implement a three-layer average:

$$\langle \Xi(z) \rangle = (\Xi(z-1) + \Xi(z) + \Xi(z+1))/3 \quad (11)$$

for some spatially dependent quantity $\Xi(z)$.

Finally, the contribution $\alpha(z)$ originates from the incompressibility constraint

$$\sum_i \varphi_i(z) = 1 \quad (12)$$

Physically, the value of $\alpha(z)$ specifies how much work it takes to generate space for the segment to be located at coordinate z (again with respect to that in the bulk). In practice, α was made more negative or less positive in an iterative way when the sum of the volume fractions was less than unity and the opposite when the volume fractions exceed unity.

The segment potentials are used in Boltzmann-like equations: defining the weighting factor $G_A(z) = \exp(-u_A(z))$, again for $A = D, W, V$. Physically these weights specify the distribution of segments A if these are not connected to other segments. Therefore, we name these weights "free segment distribution functions". Accordingly, the distribution of free volume is found from

$$\varphi_V(z) = \varphi_V^b G_V(z) \quad (13)$$

When the φ_V^b is not known, it should be computed from the incompressibility relation in the bulk $\varphi_V^b = \varphi_W^b - \varphi_D^b$.

The CO₂ molecules are composed of two monomers that occupy neighboring lattice sites on the lattice. This correlation should be accounted for in the evaluation of the volume fraction profile. The target is to compute the end-point distribution function $G_D(z, 2|1)$ as the statistical weight of finding segment $s = 2$ in coordinate z provided that it is connected to segment $s = 1$. We can compute this quantity by realizing that the first segment can be either in layer $z-1$, z or $z+1$. Averaging over these "starting" positions, we find

$$G_D(z, 2|1) = G_D(z) \langle G_D(z, 1|1) \rangle \quad (14)$$

$$G_D(z, 1|1) = G_D(z) \quad (15)$$

where $G_D(z, 1|1)$ is the statistical weight of a "walk" starting with segment $s = 1$ and ending with segment $s = 1$. As no steps are taken, we can substitute the free segment distribution function $G_D(z, 1|1) = G_D(z)$ as specified. We further realize that the volume fraction distribution of segment $s = 2$ is proportional to $G_D(z, 2|1)$

$$\varphi_D(z, 2) = C_D G_D(z, 2|1) \quad (16)$$

The total volume fraction of D should result from the sum of the distribution of the first and second segment. Realizing that

for symmetry reasons the two segments must have the same profile we find

$$\varphi_D(z) = 2\varphi_D(z, 2) = \varphi_D^b \varphi_D(z, 2) \quad (17)$$

where we have used $C_A = \varphi_A^b/N_A$ which follows from the fact that the potentials are normalized to zero in the bulk. When the bulk volume fraction φ_D^b is not known, we should know the $\theta_D = \sum_z \varphi_D(z)$ as an input quantity. We can find a value for C_D so that the summation over the profile gives θ_D .

The water molecules are seen as a star-like cluster of five W segments: one central segments and four neighbors. Let us denote one of the exterior segments as $s = 1$, the central segment as $s = 2$ and one other exterior segment as $s = 3$. Now we have three end-point distribution functions which depend recursively on each other

$$G_W(z, 3|1) = G_W(z) \langle G_W(z, 2|1)^3 \rangle / G_W(z)^2 \quad (18)$$

$$G_W(z, 2|1) = G_W(z) \langle G_W(z, 1|1) \rangle \quad (19)$$

$$G_W(z, 1|1) = G_W(z) \quad (20)$$

The top equation implements the situation that one has to combine three arms in the center in order to proceed to segment number 3. The division by $G_W(z)^2$ corrects for double counting of the statistical weight for the middle segment.

It is easily checked that for the star-like architecture the volume fraction of W follow from

$$\varphi_W(z) = C_W \left(4G_W(z, 3|1) + \frac{G_W(z, 2|1)^4}{G_W(z)^3} \right) \quad (21)$$

where the first term within the brackets gives the combined contribution of the four exterior segments and the second term is the one for the central segment. Again $C_W = \varphi_W^b/5$, and when φ_W^b is unknown, we do know the θ_W value and find the value C_W such that the profiles obeys to this.

■ THERMODYNAMIC OUTPUT PARAMETERS

Interfacial Tension. The primary results of the SCF equations are the volume fraction profiles. Then there are also the segment potentials. Using these we can accurately evaluate the Helmholtz energy F of the system. Here our interest is in the chemical potentials $\tilde{\mu}_i$ of the molecules and the grand potential $\Omega = F - \sum_i \tilde{\mu}_i n_i$ of the system, which uniquely follow from the Helmholtz energy. Note that all these quantities are normalized by L , the number of lattice sites in each layer.

The chemical potentials can conveniently be expressed using the volume fractions in the bulk $\Phi_i \equiv \varphi_i^b$ and the relation is known from the Flory–Huggins theory:

$$\begin{aligned} \frac{\tilde{\mu}_i - \tilde{\mu}_i^*}{k_B T} &= \ln \Phi_i + 1 - N_i \sum_j \frac{\Phi_j}{N_j} \\ &\quad - \frac{N_i}{2} \sum_A \sum_B (\Phi_A - \Phi_A^*) \chi_{AB} (\Phi_B - \Phi_B^*) \end{aligned} \quad (22)$$

In this equation Φ_{Ai}^* is the fraction of segments A of molecule i . As we only have segments of one type in each molecule, this value is either unity (when molecule i is composed of segments of type A) or zero (otherwise). Note that the chemical potentials are defined with respect to a reference phase, for which the pure phases (phases that are composed of only molecule i) are used. It is customary to make the chemical

potentials dimensionless, and thus we implement $\tilde{\mu}_i \equiv (\tilde{\mu}_i - \tilde{\mu}_i^*)/(k_B T)$. We will do the same, that is normalize by $k_B T$, with the grand potential.

The grand potential can be written as $\Omega \equiv (\Omega)/(k_B T) = \sum_z \omega(z)$, with $\omega(z)$ the dimensionless grand potential density (ω is equivalent with the difference between (dimensionless) tangential and normal pressures):

$$\begin{aligned} \omega(z) &= - \sum_i \frac{\varphi_i(z) - \Phi_i}{N_i} - \alpha(z) \\ &\quad - \frac{1}{2} \sum_A \sum_B \chi_{AB} (\varphi_A(z) \langle \varphi_B(z) \rangle - \Phi_A \Phi_B) \end{aligned} \quad (23)$$

where the prime indicates that in the sum only the mobile species CO_2 , water and V are included.

To obtain the interfacial tension γ from the dimensionless Ω , we use

$$\gamma = \frac{\Omega k_B T}{a^2} \quad (24)$$

and the pressure is related, as mentioned already, from the dimensionless chemical potential of the free volume component

$$P = - \frac{\tilde{\mu}_V k_B T}{a^3} \quad (25)$$

In order to calculate the IFT-pressure isotherm for a wide pressure range covering both the gas and liquid, it is necessary to treat the two phases of CO_2 (gas and liquid) separately. For the lower pressure region of the isotherm we started with a water–free volume interface and we varied the amount of CO_2 in the system, thereby changing the chemical potential of free volume, and hence the pressure. To generate the liquid branch of the isotherm, $P > P_{\text{sat}}$, we considered the water– CO_2 interface and varied the amount of free volume in the system (and hence the pressure). The effect of temperature was captured by varying the χ parameter of the system, as explained before (using eq 8).

Bulk Phase Behavior. In the case of three components, water, CO_2 and free volume (V), we can have either one homogeneous phase, three two-phase regions, or one three-phase coexistence region. For a given set of interaction parameters one can easily map out the phase diagram using the Flory–Huggins (dimensionless) Helmholtz energy density

$$f(\{\Phi\}) = \sum_i \frac{\Phi_i \ln \Phi_i}{N_i} + \frac{1}{2} \sum_A \sum_B \Phi_A \chi_{AB} \Phi_B \quad (26)$$

For phase coexistence, we require that the chemical potentials should not depend on the spatial coordinate. This means that for a given component the chemical potential is the same in each phase. This criterion is typically used to find the phase diagram. The compositions of coexisting phases fully specify all the so-called binodal values, that is, the (homogeneous) concentrations (we will use the notation $\varphi_i^\#$ for this) of all components in all coexisting phases. Our interest concerns interfacial tensions of the three interfaces, which correspond to the three possible pairs of coexisting phases. These quantities do not follow from the Flory–Huggins theory, so that we have to solve the SCF equations to find them. Interestingly, we obtain as a bonus the bulk binodals, both for

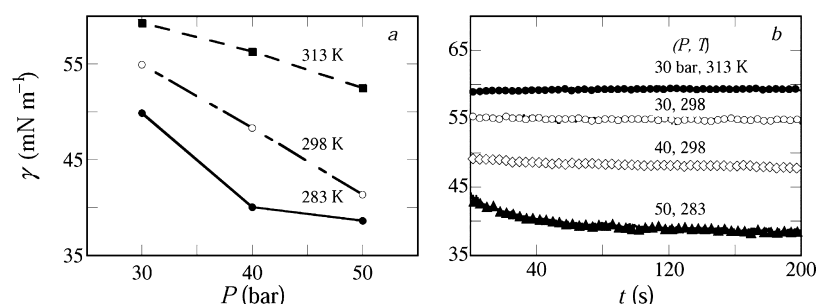


Figure 2. (a) Experimental water–CO₂ interfacial tension as a function of pressure at three different temperatures. The lines are guides to the eyes. (b) Time dependence of interfacial tension at different combinations of pressure and temperature, showing equilibration is reached within 200 s.

any of the two-phase coexistences as well as for the three-phase coexistence situation.

Contact Angle. When a macroscopic drop of one phase (liquid), surrounded by a bulk phase (gas) is placed at a substrate (solid), we may consider two situations. Either the liquid spreads along the surface and we have just two interfaces, namely solid–liquid and liquid–gas, or the liquid remains as a drop and we have three interfaces, a solid–gas, solid–liquid and liquid–gas. To maintain mechanical equilibrium there is a finite contact angle of the drop, the value of which is found from the Young equation. In the SCF theory we may study wetting phenomena, and these are most easily studied using adsorption isotherms.

SF-SCF Theory of Adsorption. In this case we consider systems that have a substrate placed at $z = 0$ as explained above. Here we focus on the adsorption of water onto the substrate. The bulk phase is either a free volume rich phase or a CO₂-rich phase. For a given amount of water in the system we first generate the volume fraction profiles ($\varphi(z)$) and from this compute the excess amount of molecules (Θ_i^{exc})

$$\Theta_i^{\text{exc}} = \sum_{z=1}^M (\varphi_i(z) - \varphi_i^{\text{b}}) \quad (27)$$

The excess number of molecules, n_i^{exc} , can then be computed by

$$n_i^{\text{exc}} = \frac{\Theta_i^{\text{exc}}}{N_i} \quad (28)$$

Water adsorption isotherms are defined as adsorbed amounts Θ_i^{exc} as a function of the bulk volume fraction of water φ_W^{b} . Of course, the bulk volume fraction (bulk concentration) is limited by the bulk binodal. For water, we denote the bulk binodal by $\varphi_W^{\#}$, where in the context it should be clear whether this is the saturation value in the free-volume rich phase or in the CO₂ rich phase.

To generate the adsorption isotherms of CO₂ at the interface between the water and free volume rich phase, a similar approach was applied. In this context we are interested in the quantity $\Theta_{\text{CO}_2}^{\text{exc}}$. From $\Theta_{\text{CO}_2}^{\text{exc}}$ it is possible to calculate the surface excess concentration of CO₂ by imagining a mathematical plane of zero thickness, known as the Gibbs plane (z^{Gibbs}) having a zero solvent (in the present case W) excess concentration.

$$z^{\text{Gibbs}} = \frac{\Theta_W^{\text{exc}}}{\varphi_W(1) - \varphi_W(M)} \quad (29)$$

The excess concentration of any solute (i) can then be found by

$$\Gamma_i = \frac{\Theta_i^{\text{exc}} - z^{\text{Gibbs}}(\varphi_i(1) - \varphi_i(M))}{N_i} \quad (30)$$

Thermodynamics: Wetting and Adsorption. It should be understood that for each value of the excess adsorbed amount we also have an accurate value for the grand potential in the system. This applies to all points of the adsorption isotherm of water on a solid substrate. Informative for wetting studies is the dependence of Ω on φ_W^{b} , or even better $\tilde{\mu}_W$. Let us first consider $\Omega(\varphi_W^{\#})$, that is the grand potential for the situation that the water component is at bulk coexistence. It turns out that when there is just one value for $\Omega(\varphi_W^{\#})$, the surface is wet by water (a macroscopic layer of the adsorbing compound is present on the surface) and when there are two distinct values, we are dealing with partial wetting. We will refer to the value of $\Omega(\varphi_W^{\#})$ for the case that Θ_W^{exc} is small with $\Omega(\text{thin})$ and for the value of $\Omega(\varphi_W^{\#})$ in the limit of $\Theta_W^{\text{exc}} \rightarrow \infty$ by $\Omega(\text{thick})$.

Following Young's equation one can write for a solid (S)–water (L)–vapor (V) system

$$\cos \theta = \frac{\gamma^{\text{SV}} - \gamma^{\text{SL}}}{\gamma^{\text{LV}}} \quad (31)$$

where, θ is the contact angle and γ^{SV} is the interfacial tension of the solid with a thinly adsorbed water film formed at the water saturated vapor pressure, and (γ^{SL} is the interfacial tension for the solid–water interface under the same conditions. Finally, γ^{LV} is the interfacial tension between water and vapor (which contains CO₂). Realizing that $\Omega(\text{thin}) = \gamma^{\text{SV}}$ and $\Omega(\text{thick}) = \gamma^{\text{SL}} + \gamma^{\text{LV}}$, we can write

$$\cos \theta = \frac{\Omega(\text{thin}) - \Omega(\text{thick})}{\gamma^{\text{LV}}} + 1 \quad (32)$$

The difference between the grand potential values of the thin and thick layer divided by the dimensionless interfacial tension of the water–CO₂ yields ($\cos \theta - 1$). From this it is trivial to extract a value for the contact angle. In this particular case the solid surface corresponds to either cellulose (hydrophilic) or HMDS (hydrophobic) modified silica surface.

RESULTS AND DISCUSSION

Experimental interfacial tension (γ) as a function of pressure (P) for water-free volume (V) systems in which CO₂ molecules are dispersed at 283, 298 and 313 K are shown in Figure 2a. The interfacial tension (γ) decreases with increasing P for all temperatures. The slope of the γ versus P isotherms increases with decreasing temperature. The temperature and pressure ranges are selected as per the requirements of dry-cleaning and

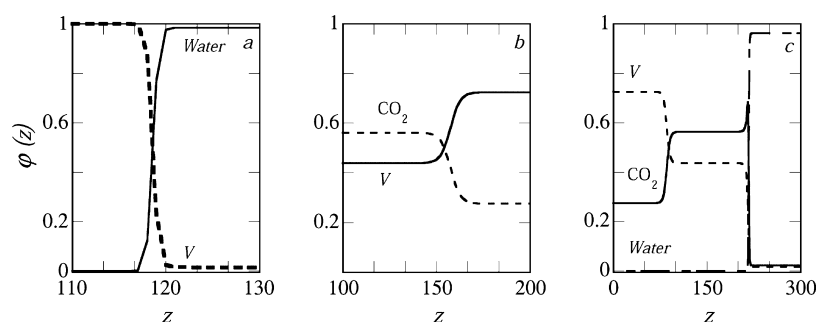


Figure 3. (a) Volume fractions of water and free volume across the binary water-free volume interface. (b) Volume fraction of CO₂ and free volume across the binary CO₂-free volume interface. (c) Volume fraction profiles of water, free volume and CO₂ at three-phase coexistence. The free-volume (V)-rich phase is on the left, the CO₂ rich phase is around $z \approx 100$ and the water-rich phase is on the right. The z -values on the x -axis are arbitrary.

to the best of our knowledge data in the literature pertaining to these conditions are either not available or sparse. Here we corrected our data by taking into account the pure CO₂ and CO₂ saturated water densities. The densities of the CO₂-rich and CO₂-saturated water-rich phases at the experimental pressures and temperatures were calculated using the equation of state of Span and Wagner³² and eqs 3 and 4 in reference.³³ The use of pure density instead of the water saturated one for the CO₂ rich phase is justified because of the extremely low solubility of water in CO₂.^{33,34} On the contrary the solubility of CO₂ in the water phase is significant, ~ 3 – 5.5% at our measurement conditions,³⁵ the density of the water phase is higher in the presence of CO₂. Moreover, the increase in water density was found to be higher in contact with gaseous CO₂ as opposed to the liquid CO₂.³³ There are many research papers dedicated to the effect of density corrections (pure phase densities versus saturated phase densities) on the IFT values of water–CO₂ mixtures. Recently it has been concluded that the use of pure phase densities leads to $>10\%$ error in the measured IFT values above 200 bar and below 343 K.³ Although we measured water–CO₂ IFT at pressures well below 200 bar we still corrected our data with the saturated phase densities of the water rich phase. The time required for the water drop to saturate with CO₂ is a subject of debate in literature.³ The effect of equilibration time on the water–CO₂ IFT values has been addressed by Bikkina et al.,⁷ who had equilibrated a water drop in CO₂ for ~ 24 h. However, the IFT reached its equilibrium value within 200 s,^{7,9} similar to our findings as shown in Figure 2b. Coming back to the results of Figure 2a, we will, in this section, delineate the molecular phenomena responsible for the decrease with γ in P . In order to do that we first look at the volume fraction profiles of W , V or/and D over the interfaces in the WV , DV and WVD systems. These are shown in Figure 3a, b and c, respectively. We see from Figure 3a and b that the W – V interface is sharper as opposed to the D – V interface, consistent with $\gamma_{\text{H}_2\text{O}-V} \gg \gamma_{\text{CO}_2-V}$. The volume fraction profiles of the phases at three phase coexistence is shown in Figure 3c. In this figure we see three phases and two interfaces. On the left there is the V -rich phase, on the right there is the water-rich phase and in between there is the CO₂ phase. We would like to draw the attention to the excess CO₂ adsorption, which shows up at the interface between water and CO₂. The bulk binodal values of the respective components can be read from the $\phi(z)$ profiles, in particular, sufficiently far away from the interfaces, e.g., at layers $z = 0, 150$, and 300 (Figure 3c). These densities are summarized in Table 2. As can be seen from Table 2 the amount of free volume in the CO₂-rich phase is 0.436, which is

Table 2. Bulk Binodal Values of CO₂, Water and Free Volume Vapor in Each Phase at 313 K for the System in Three-phase Coexistence^a

	$\phi_{\text{CO}_2}^{\#}$	$\phi_{\text{H}_2\text{O}}^{\#}$	$\phi_V^{\#}$
CO ₂	0.563	0.0005	0.436
H ₂ O	0.023	0.961	0.016
V	0.274	4.26×10^{-5}	0.725

^aThe phases rich in CO₂, water and V are labeled as CO₂, H₂O and V , respectively.

much higher than that in H₂O (0.016). Moreover, the amount of CO₂ in H₂O is 0.023, which is 2 orders of magnitude higher than the amount of H₂O in CO₂ (0.0005). Qualitatively these results were anticipated.

The CO₂–water interfacial tension is high and this triggers adsorption of CO₂ (reduction of free volume) as can be seen from Figure 3c. The much lower interfacial tension of the CO₂–vapor interface leads to no clear excess of CO₂ (Figure 3a). As long as $\gamma_{\text{H}_2\text{O}-V} < \gamma_{\text{H}_2\text{O}-\text{CO}_2} + \gamma_{\text{CO}_2-V}$ the excess of CO₂ remains finite and macroscopically one can have three interfaces in the system (namely between water and V , water and CO₂, and CO₂ and V). However, in the limit of $\gamma_{\text{H}_2\text{O}-V} \rightarrow \gamma_{\text{H}_2\text{O}-\text{CO}_2} + \gamma_{\text{CO}_2-V}$ a wetting transition occurs from whereon a macroscopically thick wetting layer of CO₂ appears between the water and vapor. In this case it is impossible to find a water–vapor interface. In our model we can easily find a CO₂ film in between the water and vapor as is shown in Figure 3c. To judge the thermodynamic stability of such a CO₂ film we need to inspect adsorption isotherms of CO₂ at the water–vapor interface corresponding to the χ parameter set described in Table 1. The adsorption isotherm shown in Figure 4 indicates that at coexistence there is indeed a macroscopic (thick) wetting layer of CO₂ at the water–vapor interface. The shape of the adsorption isotherm corresponds to the complete wetting regime.³⁶ This indicates that there are no nearby wetting transitions, consistent with the fact that the CO₂– V system is not too far from the critical point.³⁶

It is of interest to focus briefly on the surface excess of CO₂ (D) at the W – V or W – D – V interfaces shown in Figures 5a and b. Figure 5a was computed by starting with the W – V system and fixing the $\phi_{\text{CO}_2}^b$ in the water phase corresponding to the pressure and temperature conditions stated in the figure. To generate Figure 5b, we started with a W – D interface and fixed the ϕ_V^b in water at values corresponding to 140 bar and 283, 298 and 313 K. We see from Figure 5a that with increasing pressure,

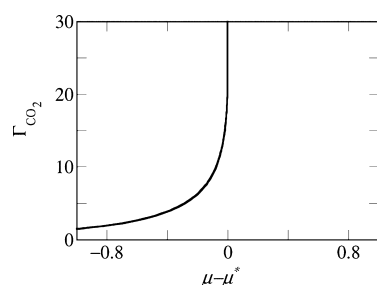


Figure 4. Gibbs excess of CO₂ at the water–V interface for the default χ parameters, that is, $\chi_{DV} = 1.5$, $\chi_{WD} = 1.5$ and $\chi_{WV} = 3.5$, showing a macroscopic thick layer of CO₂ between water–vapor interface consistent with complete wetting of the water–vapor interface by CO₂.

the Gibbs excess of CO₂ increases, even for $\varphi_{CO_2} \ll \varphi_{CO_2}^b$. Upon reaching the saturation condition and thereby having a three-phase coexistence, CO₂ continues to accumulate at the H₂O–V interface at all the three temperatures as indicated in Figure 5.

The accumulation of CO₂ at the water–vapor interface is responsible for the decrease of γ_{H_2O-V} with increasing pressure. The calculated interfacial tension between CO₂ and W with increasing CO₂ activity or P is shown in Figure 6. The value of “ a ”, the lattice parameter, as explained in Figure 1, has been chosen as 2.7 Å, to convert the grand potential (Ω) and chemical potential (μ) to interfacial tension (γ) and pressure (P) respectively (see eqs 24 and 25). For comparison, we overlay in Figure 6 the experimental γ values from our work and those obtained by other groups.¹ Not all our measured data points can be compared with literature (as the pressure and temperature ranges at which the experiments were performed were quite different), nevertheless, for some of the data points (e.g., for 298 and 313 K), there is reasonable agreement between our measurements and results of Georgiadis et al.

Figure 6 illustrates reasonable semiquantitative match between experimental and theoretical water–CO₂ interfacial tensions at three different temperatures. Although we can predict γ values for the whole pressure range we only show results up to 500 bar as the γ – P isotherms do not change much above 500 bar. With our simple mean field model all the established trends, such as the increasing slope of the γ – P isotherms with decreasing temperature and the shifting of the gas–liquid transition point (vapor pressure of CO₂) to higher pressures with increasing temperature, could be reproduced quite well even though no detailed data fitting regarding the χ parameters has been attempted.

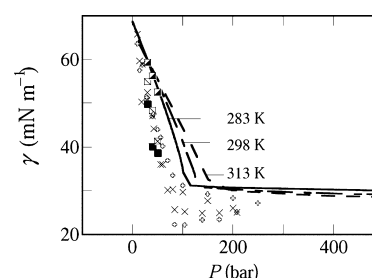


Figure 6. Comparison between experimental $\gamma_{\text{water–CO}_2}$ data and theory at 283, 298, and 313 K. The squares represent the present experimental works at 283 K (filled), 298 K (unfilled) and 313 K (half filled) respectively. The cross and plus legends represent data from literatures at 298 and 313 K respectively.¹ The curves are the interfacial tension obtained from SF-SCF modeling.

Contact Angle. Water contact angles on a hydrophilic cellulose surface immersed in CO₂ were experimentally determined as a function of pressure at 283 and 298 K (Figure 7). With increasing pressure, the contact angle increases at both temperatures indicating partial wetting of the water drop on cellulose.

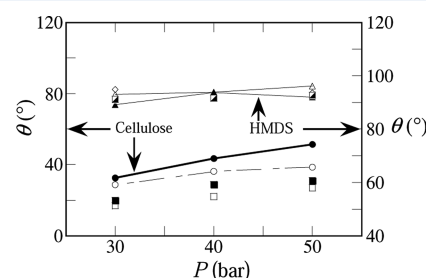


Figure 7. Comparison between experiment and modeling for water contact angle variation with pressure on cellulose (hydrophilic) and HMDS (hydrophobic) surfaces immersed in CO₂. The lines represent experimental contact angles. The filled black circles represent experimental data for cellulose at 283 K, the unfilled circles indicate experiments at 298 K, the filled and unfilled squares represent theoretical water contact angle calculated by SF-SCF theory for cellulose at 283 and 298 K, respectively. Filled and unfilled triangles correspond to experimental water contact angle on HMDS surface at 283 and 298 K, respectively. Unfilled diamond and half filled squares indicate theoretical water contact angle values on HMDS surface calculated using SF-SCF theory at 283 and 298 K, respectively.

The reason for the partial wetting could be related to the adsorption of CO₂ onto the surface –OH (hydroxyl) groups of

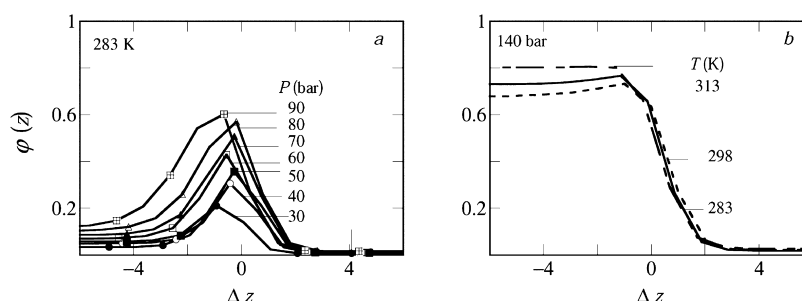


Figure 5. (a) Volume fraction profile of CO₂ across the water–V interface at 283 K and different pressures as indicated showing a Gibbs excess of CO₂ at the interface. (b) Volume fraction of CO₂ at 283, 298, and 313 K at a fixed pressure of 140 bar at the water–CO₂ interface. The excess is calculated with respect to the Gibbs dividing plane, which is at $\Delta z = 0$, Δz being $z - z^{\text{Gibbs}}$.

cellulose, thereby making the surface more hydrophobic. Similar partial wetting by water was observed on glass surfaces immersed in CO_2 .¹⁴ If this is indeed the reason, then precapping of the $-\text{OH}$ groups of hydrophilic surfaces by some alkylsilane group should result in a constant contact angle as a function of CO_2 pressure. This hypothesis was tested by measuring the water contact angle on an HMDS modified silica surface surrounded by CO_2 . The results are also shown in Figure 7. Indeed no change in contact angle was noted with increasing pressure, thus verifying our hypothesis.

It is well-known that Young's equation relates the contact angle to the respective interfacial free energies (see Figure 8), as

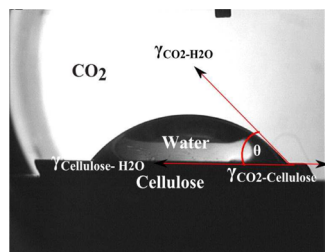


Figure 8. Water drop on a cellulose surface surrounded by CO_2 . Arrows show Young's construction of energy balance at the three-phase contact point.

given in eq 31: From Figure 2 it can be seen that $\gamma_{\text{CO}_2-\text{H}_2\text{O}}$ decreases with pressure, and provided the difference $\gamma_{\text{cellulose}-\text{CO}_2} - \gamma_{\text{cellulose}-\text{H}_2\text{O}}$ remains constant, θ should decrease. From our data in Figure 7 we see the opposite trend, that is, with increasing pressure, θ increases. So, the difference $\gamma_{\text{cellulose}-\text{CO}_2} - \gamma_{\text{cellulose}-\text{H}_2\text{O}}$ should also be pressure dependent and this we investigated by the SF-SCF theory again as presented below.

To understand the wetting characteristics of a water drop on a solid surface in CO_2 we resort to SF-SCF theory again. Modeling of contact angles requires three additional FH parameters and these are also documented in Table 1. In this case the short-range interactions with respect to the surface are attractive and defined with respect to the surface- V interaction, which was set (without loss of generality) to zero. Again we apply a flat geometry and perform a one- gradient calculation to generate the adsorption isotherms (Figures 9a and b), plotting the excess amount of water on the cellulose surface as a function of the chemical potential of water. The small oscillations in the isotherms are due to lattice artifacts.³⁸

Fortunately the oscillations are small and do not obstruct a systematic analysis.

From the adsorption isotherms it is clear that we are dealing with partial wetting, as the isotherm crosses the saturation axis at a finite (intersection between the isotherm and the saturation axis, solid black line in Figure 9) adsorbed amount, corresponding to a thin film in equilibrium with a macroscopically thick adsorbed film.³⁷ Moreover, the shaded areas r_1 and r_2 satisfy $r_1 < r_2$, Figure 9a (inset), which also indicates that we are dealing with partial wetting of the cellulose surface by the water drop.³⁷ Inspection of Figure 9 reveals that a thin (corresponding to $\Omega(\text{thin})$) and a thick film (corresponding to $\Omega(\text{thick})$) coexist at equilibrium owing to the same chemical potential ($\mu_{\text{H}_2\text{O}}$). This makes it imperative that the interface is curved, implying that it exists at the three- phase contact. To extract the contact angle from these isotherms we replot the graph as grand potential (Ω , normalized interfacial tension) versus chemical potential. The contact angle can be calculated as according to eq 32.

To model the effect of temperature on contact angle, the χ parameters can be changed as explained before. Assuming that the FH parameters are enthalpic in nature, their absolute values would decrease with temperature (eq 8). Such a scaling could explain the experimental trends of higher contact angles at lower temperature and the pressure dependence of θ for both surfaces. The modeling data are shown in Figure 7. Again we could reproduce the qualitative trends of increase of θ with pressure for the hydrophilic cellulose surface and the invariance of θ with increasing pressure for the hydrophobic HMDS surface.

Molecular-level information on how the molecules accumulate at the interface is available in the form of density (volume fraction) profiles of CO_2 , H_2O and V for various amounts of water in the system. A selection of these profiles is depicted in Figures 10, 11, 12 and 13.

From each of the adsorption isotherms shown in Figure 9, two $\Theta_{\text{H}_2\text{O}}$ values were selected namely corresponding to the thin ($\Theta_{\text{H}_2\text{O}} = 1.0 \times 10^{-5}$, Figures 10 and 11) and thick film ($\Theta_{\text{H}_2\text{O}} = 20$, Figures 12 and 13) conditions. In these figures the volume fraction profiles of the three components are given as a function of the distance from the surfaces.

Cellulose shows a stronger affinity for CO_2 (Figure 10a) as opposed to the HMDS surface (Figure 10b), whereas the opposite is noticed for the V phase. This can be explained from the difference in surface energies between cellulose and HMDS modified silica surfaces. HMDS being much more hydrophobic

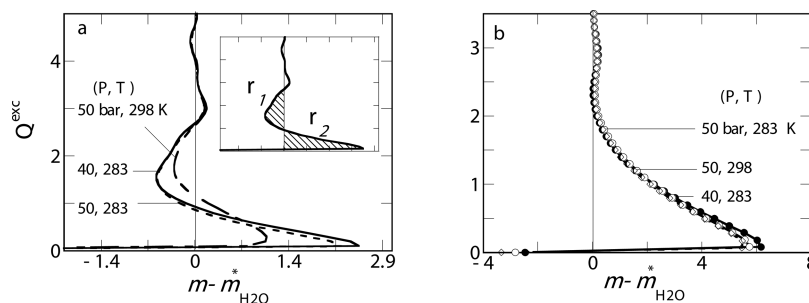


Figure 9. Calculated adsorption isotherms of water molecules on (a) cellulose and (b) HMDS surfaces immersed in CO_2 containing vapor phase at different pressures and temperatures as a function of its relative chemical potential. The shaded regions indicate partial wetting of cellulose surface by the water drop as the area $r_1 < r_2$ ³⁷ (inset, 40 bar 283 K).

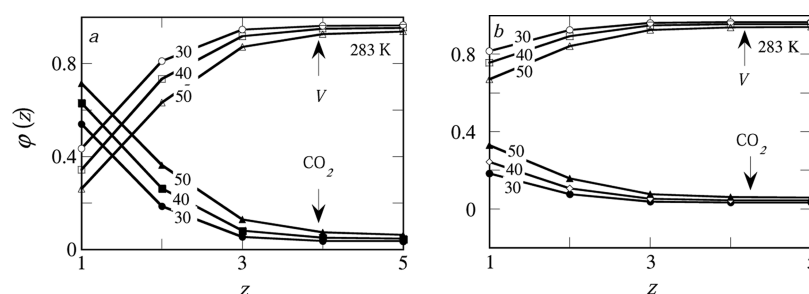


Figure 10. Calculated volume fraction profiles of CO_2 and V near (a) cellulose and (b) HMDS surfaces corresponding to a microscopic water film ($\Theta_{\text{H}_2\text{O}} = 1.0 \times 10^{-5}$). The numbers in the graphs indicate pressures.

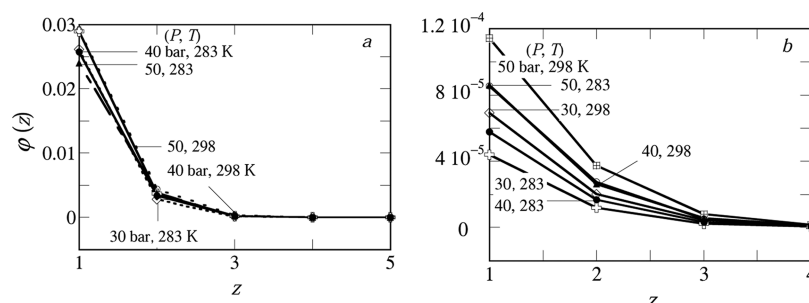


Figure 11. Calculated volume fraction profiles of H_2O near (a) cellulose and (b) HMDS surfaces corresponding to a microscopic water film ($\Theta_{\text{H}_2\text{O}} = 1.0 \times 10^{-5}$).

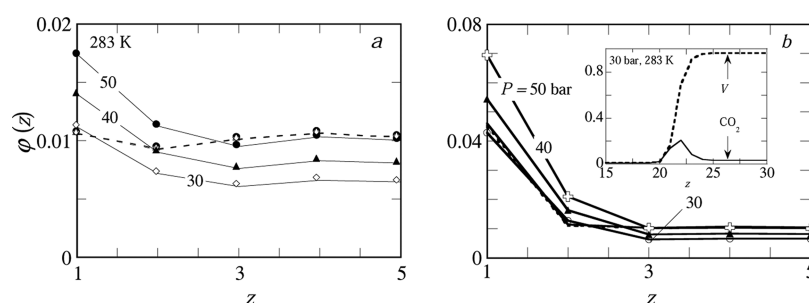


Figure 12. Calculated volume fraction profiles of CO_2 and V near (a) cellulose and (b) HMDS surfaces corresponding to a macroscopic water film ($\Theta_{\text{H}_2\text{O}} = 20$). The solid and dashed lines indicate the volume fraction profiles of CO_2 and V , respectively.

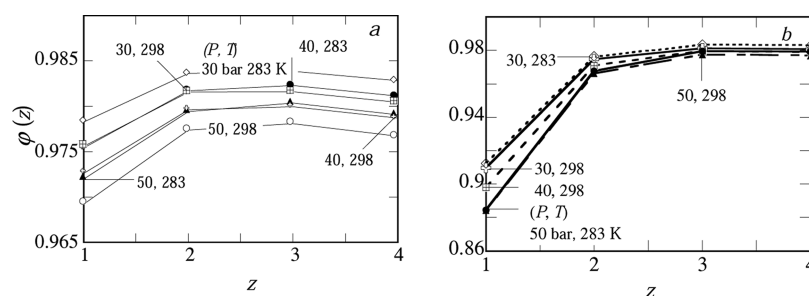


Figure 13. Calculated volume fraction profiles of H_2O near (a) cellulose and (b) HMDS surfaces corresponding to a macroscopic water film ($\Theta_{\text{H}_2\text{O}} = 20$).

(water contact angle on HMDS modified silica is $\sim 90^\circ$ compared to $\sim 30\text{--}40^\circ$ on the cellulose surface) has a stronger affinity for the V phase, whereas, cellulose having free $-\text{OH}$ groups on the surface is capable of capturing CO_2 and thereby minimizing the free energy of the system for not having to expose its hydrophilic $-\text{OH}$ groups to the V phase. Note that in the SCF model the presence of $-\text{OH}$ groups is not directly

modeled but is effectively incorporated by the FH interaction parameters.

The affinity of the cellulose surface for the CO_2 phase arguably also explains the increase of contact angle with increasing pressure. As the concentration of CO_2 in the V phase increases, the surface becomes even more covered with CO_2 , making the water drop to retract from the surface (dewetting). Water volume fraction profiles for the cellulose and HMDS

surfaces are shown in Figure 11a and b respectively at $\Theta_{\text{H}_2\text{O}} = 1.0 \times 10^{-5}$. Even at such a low water amount, the volume fraction of water near the cellulose surface is 3 orders of magnitude higher than that of the HMDS surface.

With an increased amount of water in the system ($\Theta_{\text{H}_2\text{O}} = 20$, which corresponds to $\phi_{\text{W}}^{\text{b}} \approx \phi_{\text{W}}^{\#}$), condensation of the water film has taken place on the surface, which is evident from the volume fraction profiles of water on both cellulose and HMDS surfaces as displayed in Figure 13. Here we focus on the profile near the solid phase, (small values of z), because the fluid–fluid interface (between $z = 20$ and 25 (see Figure 12b) far from the surface is identical to the free water– CO_2 interface discussed before (see Figure 5a). Interestingly, we see that the volume fraction of water decreases somewhat near the surface in favor of an increase of the free volume and CO_2 densities. This is completely in line with the finite contact angles. The higher the contact angle, the more the depletion of water and the enrichment of V and CO_2 .

CONCLUSIONS

Measurement of water-vapor interfacial tension with dispersed CO_2 in the vapor phase show that the IFT decreases with increasing pressure. Moreover, the negative slope of the IFT– P isotherm decreases with increasing temperature. These experimental findings stimulated us to model such a three-phase system to improve our molecular insight in the processes involved. We invoked a simple mean-field based approach and showed that a molecular coarse grained model based on SCF theory is sufficient for in-depth understanding of such a complex system. The SCF approach is simpler and arguably preferable over equation-of-state based models and computationally orders of magnitude less expensive than molecular dynamics simulations.

We could semiquantitatively reproduce the experimental water– V interfacial tension at 283, 298 and 313 K with dispersed CO_2 phase by incorporating suitable FH parameters into the model. Our modeling results point toward the presence of a surface excess of CO_2 at both the H_2O – V interface and at the three phase coexistence region. The adsorption isotherms of CO_2 point toward the existence of a wetting film of CO_2 at the W – V interface for all the conditions. The trends in the water contact angle on cellulose and HMDS surfaces were also successfully modeled and the volume fraction profiles of all the three phases near the surfaces and at bulk were constructed, which show that the hydrophilic cellulose surface irrespective of the water amount in the system, prefers to have CO_2 molecule on its surface over the free volume phase. This phenomenon could be responsible for the increase of contact angle of water with increasing pressure on the cellulose surface.

In a follow-up study, we will extend this type of mean field model toward the understanding of phase behavior of CO_2 -soluble surfactants in multi component systems.

ASSOCIATED CONTENT

Supporting Information

Infrared reflection absorption spectroscopy (IRRAS) data of the HMDS-modified and unmodified Silicon wafers (Scheme 14) to show that after the modification, the HMDS surface is methyl rich due to the formation of $-\text{OSi}(\text{CH}_3)_3$ from $-\text{SiOH}$. This material is available free of charge via the Internet at <http://pubs.acs.org>.

AUTHOR INFORMATION

Corresponding Author

*E-mail: soumi.banerjee@wur.nl, frans.leermakers@wur.nl.
Phone: +31(0)317483543, +31(0)317-482268.

Notes

The authors declare no competing financial interest.

ACKNOWLEDGMENTS

S.B. and F.L. thank Prof. Rudolf Eggers and Dr. Philip Jaeger of the Technical University Hamburg-Harburg for facilitating the experimental works and helpful discussions. This research is supported by the Dutch Technology Foundation STW, which is the applied science division of the Dutch Scientific Organisation NWO, and the Technology programme of the Ministry of Economic Affairs.

REFERENCES

- (1) Georgiadis, A.; Maitland, G.; Trusler, J. P. M.; Bismarck, A. Interfacial Tension Measurements of the $\text{H}_2\text{O}+\text{CO}_2$ System at Elevated Pressures and Temperatures. *J. Chem. Eng. Data* **2010**, *5*, 4168–4175.
- (2) Lafitte, T.; Mendiboure, B.; Piñeiro, M. M.; Bessières, D.; Miqueu, C. Interfacial Properties of Water/ CO_2 : A Comprehensive Description through a Gradient Theory-SAFT-VR Mie Approach. *J. Phys. Chem. B* **2010**, *114*, 11110–11116.
- (3) Nielsen, L. C.; Bourg, I. C.; Sposito, G. Predicting CO_2 -Water Interfacial Tension Under Pressure and Temperature Conditions of Geologic CO_2 Storage. *Geochim. Cosmochim. Acta* **2011**, *81*, 28–38.
- (4) Banerjee, S.; Sutanto, S.; Kleijn, J. M.; van Roosmalen, M. J. E.; Witkamp, G. J.; Cohen Stuart, M. A. Colloidal Interactions in Liquid CO_2 - A Dry-cleaning Perspective. *Adv. Colloid Interface Sci.* **2012**, *175*, 11–24.
- (5) Blunt, M.; John Fayers, F.; Orr, F. M. Carbon Dioxide in Enhanced Oil Recovery. *Energy Convers. Manage.* **1993**, *34*, 1197–1204.
- (6) McHugh, M. A.; Krukonis, V. J. *Supercritical Fluid Extraction. Principles and Practice*; Butterworth Publishers: Stoneham, MA, 1986.
- (7) Bikkina, P. K.; Shoham, O.; Uppaluri, R. Equilibrated Interfacial Tension Data of the CO_2 -Water System at High Pressures and Moderate Temperatures. *J. Chem. Eng. Data* **2011**, *56* (10), 3725–3733.
- (8) Chun, B.-S.; Wilkinson, G. T. Interfacial Tension in High-Pressure Carbon Dioxide Mixtures. *Ind. Eng. Chem. Res.* **1995**, *34*, 4371–4377.
- (9) Hebach, A.; Oberhof, A.; Dahmen, N.; Kogel, A.; Ederer, H.; Dinjus, E. Interfacial Tension at Elevated Pressures Measurements and Correlations in the Water + Carbon Dioxide System. *J. Chem. Eng. Data* **2002**, *47*, 1540–1546.
- (10) Chiquet, P.; Daridon, J. L.; Broseta, D.; Thibeau, S. CO_2 /water Interfacial Tensions under Pressure and Temperature Conditions of CO_2 Geological Storage. *Energy Convers. Manage.* **2007**, *48*, 736–744.
- (11) Kvamme, B.; Kuznetsova, T.; Hebach, A.; Oberhof, A.; Lunde, E. Measurements and Modelling of Interfacial Tension for Water+Carbon Dioxide Systems at Elevated Pressures. *Comput. Mater. Sci.* **2007**, *38*, 506–513.
- (12) Bachu, S.; Bennion, D. B. Interfacial Tension between CO_2 , Freshwater, and Brine in the Range of Pressure from (2 to 27) MPa, Temperature from (20 to 125) °C, and Water Salinity from (0 to 334000) mg/L. *J. Chem. Eng. Data* **2009**, *54*, 765–775.
- (13) Sutjiadi-Sia, Y.; Jaeger, P.; Eggers, R. Interfacial Phenomena of Aqueous Systems in Dense Carbon Dioxide. *J. Supercrit. Fluids* **2008**, *46*, 272–279.
- (14) Dickson, J. L.; Gupta, G.; Horozov, T. S.; Binks, B. P.; Johnston, K. P. Wetting Phenomena at the CO_2 /Water/Glass Interface. *Langmuir* **2006**, *22*, 216–2170.
- (15) Monte Carlo Simulation of H_2O - CO_2 Mixtures to 1073.15 K and 30 kbar. *Chem. Geol.* **1996**, *133*, 53–65.

- (16) Panhuis, P. C. H.; M. H.; Lynden-Bell, R. M. A Molecular Dynamics Study of Carbon Dioxide in Water: Diffusion, Structure and Thermodynamics. *Mol. Phys.* **1998**, *94*, 963–972.
- (17) Zhang, Z.; Zhenhao, D. An Optimized Molecular Potential for Carbon Dioxide. *J. Chem. Phys.* **2005**, *122*, 214507–214522.
- (18) Kuznetsova, T.; Kvamme, B. Thermodynamic Properties and Interfacial Tension of a Model Water-Carbon Dioxide System. *Phys. Chem. Chem. Phys.* **2002**, *4*, 937–941.
- (19) Zhao, L.; Lin, S.; Mendenhall, J. D.; Yuet, P. K.; Blankschtein, D. Molecular Dynamics Investigation of the Various Atomic Force Contributions to the Interfacial Tension at the Supercritical CO₂-Water Interface. *J. Phys. Chem. B* **2011**, *115*, 6076–6087.
- (20) Cahn, J. W.; Hilliard, J. E. Free Energy of a Nonuniform System. I. Interfacial Free Energy. *J. Chem. Phys.* **1958**, *28*, 258–267.
- (21) Nino-Amezquita, O. G.; Enders, S.; Jaeger, P. T.; Eggers, R. Measurement and Prediction of Interfacial Tension of Binary Mixtures. *Ind. Eng. Chem. Res.* **2010**, *49*, 592–601.
- (22) Evers, O. A.; Scheutjens, J. M. H. M.; Fleer, G. J. Statistical Thermodynamics of Block Copolymer Adsorption. I. Formulation of the Model and Results for the Adsorbed Layer Structure. *Macromolecules* **1990**, *23*, 5221–5233.
- (23) Evers, O. A.; Scheutjens, J. M. H. M.; Fleer, G. J. Statistical Thermodynamics of Block Copolymer Adsorption. Part 2.-Effect of Chain Composition on the Adsorbed Amount and Layer Thickness. *J. Chem. Soc., Faraday Trans.* **1990**, *86*, 1333–1340.
- (24) Flory, P. J. Thermodynamics of High Polymer Solutions. *J. Chem. Phys.* **1941**, *9*, 660–660.
- (25) Banerjee, S.; Mulder, P.; Kleijn, J. M.; Cohen Stuart, M. A. Effect of Surface Roughness and Softness on Water Capillary Adhesion in Apolar Media. *J. Phys. Chem. A* **2012**, *116*, 6481–6488.
- (26) Kontturi, E.; Thüne, P. C.; Niemantsverdriet, J. W. Cellulose Model Surfaces: Simplified Preparation by Spin Coating and Characterization by X-ray Photoelectron Spectroscopy, Infrared Spectroscopy, and Atomic Force Microscopy. *Langmuir* **2003**, *19*, 5735–5741.
- (27) Hill, T. L. *An Introduction to Statistical Thermodynamics*, 3rd ed.; Addison-Wesley: Boston, 1960.
- (28) Postmus, B. R.; Leermakers, F. A. M.; Cohen Stuart, M. A. Self-Consistent Field Modeling of Poly(ethylene oxide) Adsorption onto Silica: The Multiple Roles of Electrolytes. *Langmuir* **2008**, *24*, 1930–1942.
- (29) Leermakers, F. A. M.; Scheutjens, J. M. H. M. Statistical Thermodynamics of Association Colloids: V. Critical Micelle Concentration, Micellar Size and Shape. *J. Colloid Interface Sci.* **1990**, *136*, 231–241.
- (30) Jødar-Reyes, A. B.; Ortega-Vinuesa, J. L.; Martín-Rodríguez, A.; Leermakers, F. A. M. Modeling the Effect of Structural Details of Nonionic Surfactants on Micellization in Solution and Adsorption onto Hydrophobic Surfaces. *Langmuir* **2002**, *18*, 8706–8713.
- (31) Scheutjens, J. M. H. M.; Fleer, G. J. Statistical Theory of the Adsorption of Interacting Chain Molecules. I. Partition Function, Segment Density Distribution, and Adsorption Isotherms. *J. Phys. Chem.* **1979**, *83*, 1619–1635.
- (32) Span, R.; Wagner, W. A New Equation of State for Carbon Dioxide Covering the Fluid Region from the Triple-Point Temperature to 1100 K at Pressures up to 800 MPa. *J. Phys. Chem. Ref. Data* **1996**, *25*, 1509–1596.
- (33) Hebach, A.; Oberhof, A.; Dahmen, N. Density of Water + Carbon Dioxide at Elevated Pressures: Measurements and Correlation. *J. Chem. Eng. Data* **2004**, *49*, 950–953.
- (34) King, M. B.; Mubarak, A.; Kim, J. D.; Bott, T. R. The Mutual Solubilities of Water with Supercritical and Liquid Carbon Dioxides. *J. Supercrit. Fluids* **1992**, *5*, 296–302.
- (35) Duan, Z.; Sun, R. An Improved Model Calculating CO₂ Solubility in Pure Water and Aqueous NaCl Solutions from 273 to 533 K and from 0 to 2000 bar. *Chem. Geol.* **2003**, *193*, 257–271.
- (36) Cahn, J. W. Critical Point Wetting. *J. Chem. Phys.* **1977**, *66*, 3667–3672.
- (37) Derjaguin, B. V.; Churaev, N. V.; Muller, V. M. *Surface Forces*; Plenum Press: New York, 1960.
- (38) Schlangen, L.; Leermakers, F. A. M.; Koopal, L. K. Self-Consistent Field Theory for Wetting of Binary Polymer-Solvent Mixtures on Rigid and Soft Interfaces. *J. Chem. Soc., Faraday Trans.* **1996**, *92*, 579–587.